This document is the accepted manuscript version of the following article:
Maluk, C., Bisby, L., & Terrasi, G. P. (2022). Thermal incompatibility between CFRP tendons and concrete. Journal of Composites for Construction, 26(6), 04022080 (13 pp.). https://doi.org/10.1061/(ASCE)CC.1943-5614.0001260

Thermal incompatibility between CFRP tendons and concrete

Cristian Maluk [1,2], Luke Bisby [3], and Giovanni P. Terrasi [4]

[1] Senior Lecturer, School of Civil Engineering, The University of Queensland, Australia
Advanced Engineering Building, Staff House Road, St. Lucia, 4072 Australia
c.maluk@uq.edu.au

[2] Technical Director, Semper, UK
3, Waterhouse Square, 138 Holborn, London EC1N 2SW, United Kingdom

[3] School of Engineering, The University of Edinburgh, UK
William Rankine Building, The King's Buildings, Edinburgh, EH9 3FB, UK
luke.bisby@ed.ac.uk

[4] EMPA Dübendorf, Zurich, Switzerland
EMPA, Überlandstrasse 129, Dübendorf, Uster, CH-8600, Switzerland
giovanni.terrasi@empa.ch

Abstract:

Results are presented from a comprehensive experimental study to assess the occurrence of heat-induced longitudinal splitting cracks in concrete specimens reinforced with CFRP or steel when exposed to severe heating from one side, as would likely occur in a fire in a building. Tests were performed on large- and medium-scale precast CFRP reinforced or prestressed specimens. Large-scale specimens were tested in a standard fire resistance test, while medium-scale specimens were tested using a novel Heat-Transfer Rate Inducing System (H-TRIS) which controls thermal exposure by imposing a time-history of incident heat flux at a specimen's exposed surface. The formation of thermally induced longitudinal splitting cracks and failure of the concrete cover to provide sufficient confining action, and thus sufficient bond strength, is shown to be more likely for FRP reinforced or

prestressed concrete elements than for those reinforced or prestressed with steel. This appears to be at least partly due to thermo-mechanical incompatibility between CFRP reinforcement and concrete; formation of heat-induced longitudinal splitting cracks is related to rapid thermal expansion of CFRP tendons relative to the surrounding concrete. Many aspects of bond performance at elevated temperature remain poorly understood, and these require additional investigation before FRP reinforced or prestressed elements can be used in fire-rated applications with confidence.

Keywords:
CFRP; concrete; thermal expansion; longitudinal splitting cracks; H-TRIS; furnace test; analytical modelling.

Introduction and Background

Driven by the need for more durable and sustainable concrete structures, careful selection, design, and optimization of both the concrete mixes and the reinforcing materials used are now commonplace within the precast concrete industry (Terrasi et al. 2012). For example, structural elements incorporating high-performance, self-consolidating concrete (HPSCC) and carbon fibre reinforced polymer (CFRP) allow for a reduced concrete cover and overall thickness while providing excellent serviceability (corrosion resistance, high stiffness and fatigue strength). Such elements represent the forefront of innovation within the precast concrete industry; however, they also present challenges in applications where structural fire resistance must be considered.

Minimum concrete cover to traditional steel reinforcing bars or to prestressed steel wires in concrete elements is commonly limited in design, primarily by considerations related to electrochemical corrosion (CEN 2004a). Avoiding corrosion of steel is thus a key challenge for the concrete industry (Mehta 1997). Whilst sufficient concrete cover is also required for adequate fire resistance and to allow development of reinforcement stresses through bond (i.e. confinement), these additional issues are rarely explicitly considered by practicing structural engineers. Given their resistance to electrochemical corrosion, fibre reinforced polymers (FRPs) provide a good alternative to steel as internal reinforcement for concrete structures in many applications. Considerable advantages in terms of high strength-to-weight ratios, high stiffness-to-weight ratios, and magnetic neutrality (useful in certain

medical and communications infrastructure applications) have also promoted the use of FRP (Burgoyne 1997). However, before FRP reinforcement or prestressing can be used with the confidence with which steel reinforcements are applied, the behaviour of FRP under the full range of possible conditions must be first properly understood and accounted for in design.

Differences in the constituent materials used in FRP bar manufacture yield considerable differences in stiffness, strength, and bond behaviours of commercially available FRP bars and prestressing tendons. A range of different fibres are used, the most common being carbon in FRP prestressed concrete applications. In CFRP prestressing strands or tendons, the carbon fibres may occupy between 30% and 70% of the overall volume of the bars – the remainder being polymer resin matrix, which binds the fibres together. The longitudinal tensile strength and stiffness of FRP tendons is highly dependent on the type of fibre and fibre-volume fraction. Glass fibre reinforced polymers (GFRPs) commonly have a larger nominal mass, and the critical disadvantage of a comparatively low creep-rupture and alkaline stress corrosion resistance, making them unsuitable for most prestressing applications. Carbon fibre reinforced polymers (CFRPs) have comparatively high tensile strength and stiffness as compared with other commonly used FRPs (Balafas and Burgoyne 2012) and have excellent resistance to creep deformation and relaxation (Seica and Packer 2007). Thus, CFRP is the FRP of choice for prestressing tendons for concrete. Epoxies and vinylesters are the most commonly used polymer resin matrices used for manufacturing CFRP prestressing tendons.

Fibre reinforced polymer tendons are typically produced using the pultrusion process (Clarke 1993); the disadvantage of this approach is that pultruded sections have a smooth surface that is undesirable for developing a strong bond (i.e. load transfer) within concrete. A secondary process is therefore typically required during the pultrusion process, in which a continuous coating of adhesive resin and fibres and/or sand is laid down on the bar's surface, thus providing a surface texture to promote bond. The bond strength of FRP tendons is therefore widely considered to rely on the strength and stiffness of the polymer resin matrix at the bars' surface, which may incorporate a sand coating, spiral fibre rovings, and/or a ribbed shaped resin surface.

Prior research has shown that the fire-performance of FRP reinforced or prestressed concrete elements is critically related to degradation of the bond between FRP tendons and concrete at elevated temperature; i.e. softening of the coating of the tendon as the polymer resin undergoes a glass transitioning process (Bisby et al. 2005). An

indirect influence due to the thermo-mechanical incompatibility (i.e. dissimilar thermal expansion) between orthotropic FRP tendons and concrete has also been considered in early research into the use of FRP reinforcement for concrete (Gentry and Bank 1994, Terrasi 1998), leading to the minimum concrete cover requirements for FRP bars within concrete; however this has not received much attention in recent years, is not directly applicable to prestressing (as opposed to reinforcing) applications, and never before considered the extreme thermal gradients that are likely to be experienced during fire exposures in buildings (or during standard fire tests). Differential thermal expansion between FRP and concrete may lead to the development of heat-induced longitudinal splitting cracks along FRP bars and tendons, and eventually to loss of the concrete cover's ability to provide sufficient confining action for bond to be maintained (Terrasi et al. 2012). The bond strength reductions resulting from softening of the polymer resin of FRP tendons at elevated temperature are widely considered to be the limiting factor in the fire-safe application of FRP reinforced or prestressed concrete (Katz et al. 1999, Bisby and Kodur 2007). The glass transition temperature (T_g) of an FRP's polymer resin is therefore widely used to define the limiting temperature for FRP materials (CNR 2006, ACI 2015), yet the research to support such an approach is rather limited in scale and scope.

Research Significance

FRP tendons have markedly different coefficients of thermal expansion (CTEs) in the longitudinal and transverse directions, and these also differ substantially from concrete or reinforcing steel. For example, pultruded CFRP tendons typically have very low (or even negative) CTEs in their longitudinal direction, since the CTE longitudinally is governed by the CTE of the carbon fibres, which is low (less than 2×10^{-7} mm/mm °C) or even slightly negative. In the transverse direction CFRP's CTEs are governed by their polymer matrices (ACI 2015) and are typically larger by an order of magnitude.

Prior studies (mostly theoretical rather than experimental) have been performed to attempt to understand the possible consequences of differential thermal expansion between FRP bars/tendons and surrounding concrete under uniform and mild heating, since this was thought to contribute to generation of longitudinal splitting cracks and loss of confining action for tensile bond development and force transfer (Gentry and Bank 1994, Matthys et al. 1996, Aiello 1999, Masmoudi et al. 2005, Abdalla 2006). The potential for differential thermal expansion to

lead to splitting cracks and loss of confinement under extreme heating and steep thermal gradients, as would occur in a fire, has not yet been investigated. The research described herein studied the appearance of heat-induced longitudinal splitting cracks in thin-walled precast CFRP prestressed concrete elements during fire, to shed light on this potentially important failure mode for FRP reinforced or prestressed concrete elements during fire. Broader consequences for the fire-safe design of FRP reinforced or prestressed concrete are also discussed.

Experimental Programme

The overall experimental programme, aspects of which have been presented in detail elsewhere (Maluk 2014), included heating tests of large- and medium-scale CFRP reinforced or prestressed concrete specimens. A series of large-scale furnace tests (summarized below) were previously performed on loaded CFRP prestressed HPSCC concrete flexural elements (Terrasi et al. 2012). These tests were expected to show that the temperature of the FRP reinforcement at the prestress transfer zone (at the ends of the specimens) would be the critical parameter influencing the fire performance of the prestressed concrete elements during fire, and that the bond between the CFRP tendons and the concrete would fail at temperatures in the region of the polymer resin's glass transition temperature but would otherwise be maintained at lower temperatures. These tests demonstrated, however, that longitudinal splitting cracks formed in the anchorage zones of the prestressed FRP tendons, leading to bond failure at lower temperatures than was expected on the basis of the known T_g of the FRP bars.

Test Specimens

The CFRP prestressed or reinforced concrete specimens tested within this study all had a rectangular cross section with a depth of either 45 mm (1.77 in.) or 60 mm (2.36 in.) and a width of 200 mm (7.87 in.). Prestressing tendons (either CFRP bars or steel prestressing wires) were placed at the specimens' mid-depth (with a tolerance of ±2 mm (0.08 in.)), corresponding to clear concrete covers to the prestressed CFRP reinforcement of 19.5 mm (0.77 in.) or 27 mm (1.06 in.). The lateral concrete cover to the specimen edges was 22 mm (0.87 in.) in all cases, with tendon-to-tendon clear spacing of 44 mm (1.73 in.). The cross section of a typical 45 mm (1.77 in.) thick specimen is shown in Figure 1.

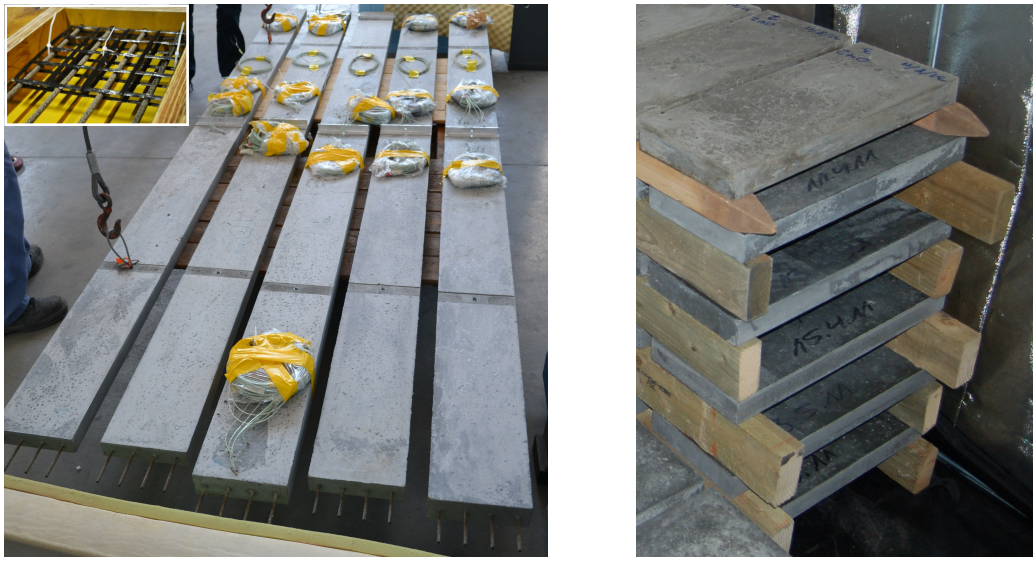

Figure 1 – Photos showing 3355 mm (11.01 ft.) long large-scale specimens and 500 mm (19.69 in.) long medium-scale specimens before testing. CFRP grids located, before casting, at the prestress transfer zones of large-scale specimens are shown at the top-left corner of the figure.

The large-scale prestressed test specimens testing in fire testing furnaces had an overall length of 3355 mm (11.01 ft.), width of 200 mm (7.87 in), and a thickness of 45 or 60 mm (1.77 or 2.36 in.). CFRP grids were placed within the prestress transfer zones of some of the specimens (see Figure 1), both above and below the prestressed CFRP tendons, in an attempt to improve the bond strength of some of the tested specimens by limiting the formation of splitting cracks in the prestress transfer zones (that had been observed in earlier large-scale tests (Terrasi et al. 2012)). These CFRP grids had transverse and longitudinal spacings of 46 mm (1.81 in.) and 41 mm (1.61 in.) respectively, with a design tensile elastic modulus of approximately 120 GPa (17,404 ksi) in both directions.

The medium-scale, unstressed test specimens tested using the H-TRIS apparatus had an overall length of 500 mm (19.69 in.) and a thickness of 45 mm (1.77 in.). In structural fire resistance testing scaling may be important on various grounds, both thermal and structural (Harmathy and Lie 1970); hence, the cross-section of the medium-scale specimens was not scaled relative to the large-scale specimens. Medium-scale specimens contained four unstressed CFRP tendons or steel wires positioned in the same configuration as in the large-scale specimens (i.e. as in Figure 2). Mixing, casting and curing of all test specimens were performed according to real industry manufacturing standards.

175 *Figure 2 – Cross section of a 45 × 200 mm2 (1.77 × 7.87 in. 2) test specimen, showing concrete covers and*
176 *location of CFRP tendons.*

177

178 **Constituent Materials**

179

180 *CFRP prestressing tendons* — Round, commercially available sand-coated CFRP prestressing tendons[1],
181 Switzerland, were used in this study. The carbon fibre volume fraction was 62% and the bars had an epoxy
182 polymer resin matrix. The CFRP tendons were 5.4 mm (0.213 in.) in nominal diameter and were fabricated by the
183 pultrusion process (ACI 2015). The CFRP tendons have a sand coating applied to the surface by broad-casting
184 silica sand into a coating of epoxy resin applied after the primary pultrusion and curing processes. The sand coating
185 is part of the standard manufacturing process for this type of CFRP tendons; this provides mechanical bond
186 between the tendon and surrounding concrete. The sand coating was approximately 0.3 mm (0.012 in.) thick. The
187 manufacturer specified nominal tensile strength of the CFRP was 2000 MPa (290 ksi) with a nominal elastic
188 modulus of 150 GPa (21,756 ksi) and an ultimate strain of 1.33%. The CFRP bars had a nominal mass of 44 gr/m
189 (5.09 oz/ft), which is only 20% that of steel prestressing. The CFRP tendon and steel prestressing wire used in the
190 current study are both shown in Figure 3.

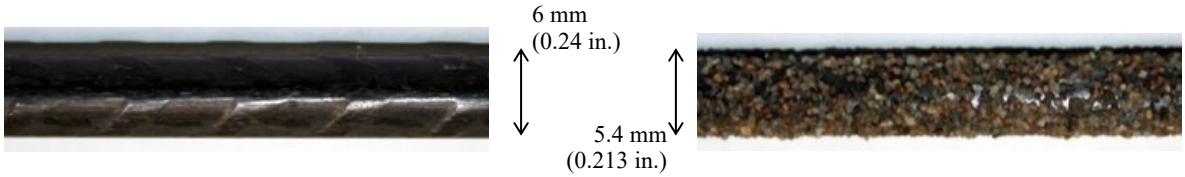

191

192 *Figure 3 – Ribbed steel prestressing wire (left) and sand-coated CFRP prestressing tendon (right) used in the*
193 *current study (diameter of wire and tendon are shown in the figure).*

194

[1] Specific CFRP and steel prestressing tendon suppliers are noted solely for the purposes of factual accuracy.

Coefficient of thermal expansion (CTE) measurements were performed on the CFRP tendons; these were carried out in accordance with applicable ASTM (2019) standards over a temperature range from 20 to 260°C (68 to 500°F). Decomposition of the CFRP's epoxy resin matrix was observed at temperatures exceeding 260°C (500°F). The measured thermal elongation ($\Delta l/l$) of the CFRP in the transverse and longitudinal directions is shown in Figure 4. This figure also shows theoretical thermal elongation curves for prestressing steel and concrete (assumed with siliceous aggregate) prescribed by design guidelines (CEN 2004b). The results show that while the free CTE of the CFRP tendons in the longitudinal direction is very low, and reasonably similar to that for concrete and prestressing steel, it is an order of magnitude higher in the transverse direction.

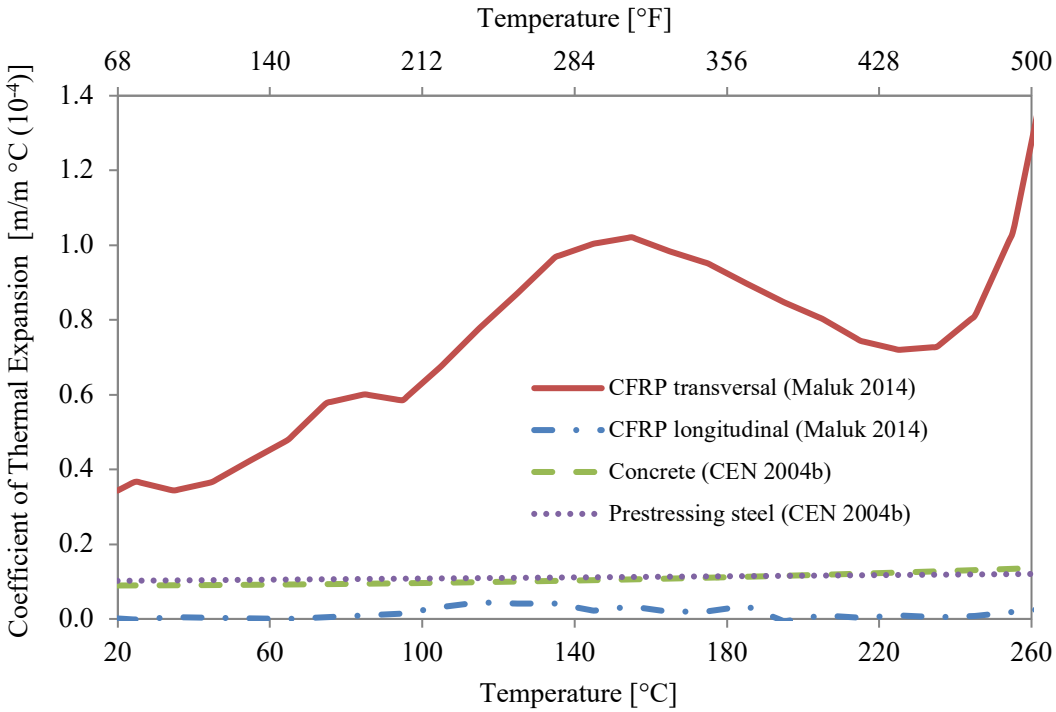

Figure 4 – Coefficients of thermal expansion for concrete, CFRP (measured transversal and longitudinal), and steel (code-prescribed).

The diameter of CFRP tendons used was defined on the basis investigations of available pultrusion diameters (4, 5.4 or 6.5 mm diameter tendons). The diameter of CFRP tendons aimed at being (1) large enough to achieve a tendon cross section having a reasonable capacity for prestress force applied per tendon; between 23 and 27.5 kN and (2) small enough to avoid longitudinal prestress transfer cracks when pretensioning, considering that the depth of elements (and therefore concrete cover to the tendon) needed to remain as low as possible. The small size of CFRP tendon diameter used (5.4 mm) was expected to also avoid the occurrence of longitudinal splitting cracks

213 during heating due to thermal expansion incompatibility between concrete and CFRP tendons in the transverse
214 direction; this is explained in depth later in this article.
215
216 *Steel prestressing wire* — For comparison against conventional prestressing materials, deformed (ribbed) steel
217 prestressing wire, produced specifically for prestressing applications by NEDRI Spanstaal BV, Netherlands, was
218 also used as internal reinforcement in comparator specimens. The steel prestressing wire was nominally 6 mm
219 (0.24 in.) in diameter with a nominal mass of 221 gr⁄m (25.58 oz/ft). The manufacturer's specified design yield
220 strength (0.2% offset) was 1592 MPa (231 ksi) and the ultimate strength was 1770 MPa (257 ksi). The elastic
221 modulus was 210 GPa (30,458 ksi). The 0.2% offset yield strain was 0.76% and the ultimate strain was 5.4%. The
222 steel wire is shown in Figure 3.
223
224 *Concrete (HPSCC)* — The high performance and comparatively high cost of CFRP prestressing requires a
225 correspondingly high-quality concrete mixture to justify use of CFRP prestressing tendons. A high performance,
226 self-consolidating concrete (HPSCC) with a 28-day minimum cube strength of 90 MPa (13.1 ksi) was used in this
227 study. This mix is representative of those currently being used within the precast industry in Europe. The concrete
228 mix included normal Portland cement, silica fume, fly ash, super-plasticizer, and a precise grain size distribution
229 of selected 0-8 mm (0-0.315 in.) limestone aggregates (refer to Table 1). Details of the granulometry for
230 aggregates used is described in detail elsewhere (Maluk 2014). Additionally, 3 or 6 mm (0.12 or 0.24 in.) long
231 monofilament polypropylene (PP) fibres were included in mixes A and B, respectively.

Large-scale fire test

Test setup — Five large-scale, CFRP prestressed concrete specimens were tested, simultaneously, in a standard furnace test (a.k.a. standard fire resistance test) (see Figure 5). The standard furnace test was programmed to follow the standard time-temperature curve (CEN 2020). It is noteworthy that the sides of the specimens were fully insulated during testing so that thermal exposure was on their bottom surfaces only. Since no clear influence of an unheated overhang length in excess of 160 mm (6.30 in.) was seen in similar fire resistance tests performed between 2009 and 2010 (Terrasi et al. 2012), all large-scale specimens had a constant unheated overhang length of 195 mm (7.68 in.) outside the furnace (Figure 6), resulting in a fire-exposed span length of 2965 mm (9.73 ft.).

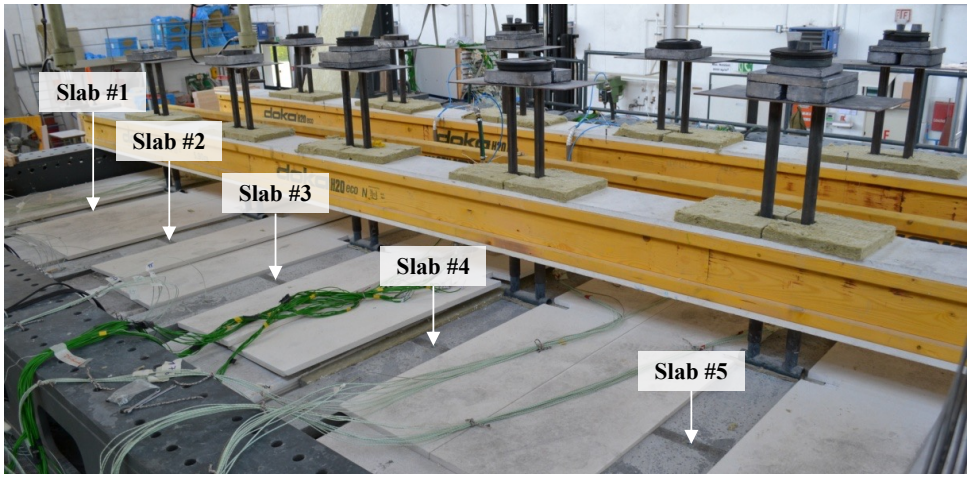

Figure 5 – Photo of the fire resistance test setup showing the positions of the large-scale specimens on the top of the fire testing furnace (spaces between the test specimens were filled-in with insulating boards).

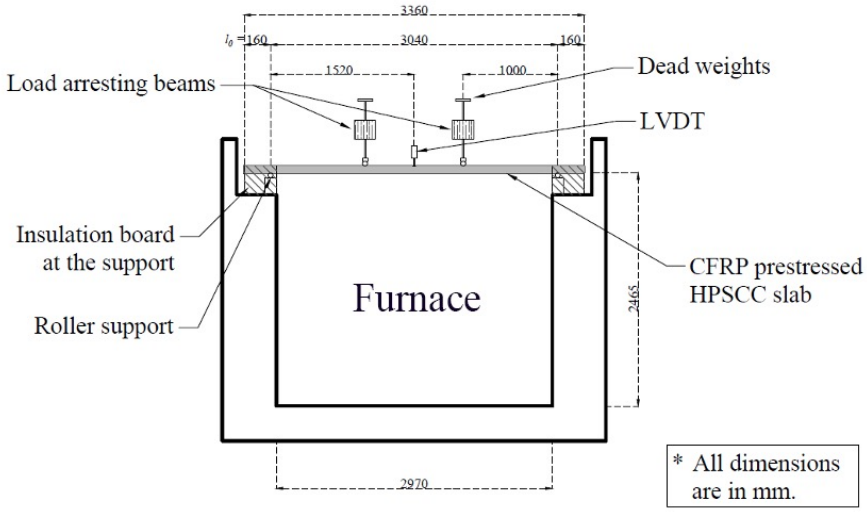

Figure 6 – Layout and test setup for the large-scale fire resistance tests (plan and side elevation views) (after Terrasi et al. 2012).

The simply supported specimens were mechanically loaded in four-point bending during testing (Figure 6). Mechanical loading was defined so as to achieve decompression at the tension fibre within the constant moment region. This corresponds to a typical design service load condition for a CFRP prestressed façade element in a real building (Terrasi 2007). The applied load was calculated considering the age dependency of the prestressing losses due to elastic shortening, shrinkage and creep effects, resulting in applied loads (per point) of 25.0 kg (55.1 lb) and 38.4 kg (84.7 lb) for specimens 45 mm (1.77 in.) and 60 mm (2.36 in.) thick, respectively. The applied loading conditions was decided based on manufacturer's design service conditions.

Table 1 – Concrete mix compositions and slump flow measurements.

Mix Label	Water/ (cement + micro silica + fly ash) [-]	Cement [kg/m^3] [lb/ft^3]	Fly ash [kg/m^3] [lb/ft^3]	Limestone aggregate [kg/m^3] [lb/ft^3]	Super-plasticizer [% of cement]	Dose of PP fibres [kg/m^3] [lb/ft^3]	Slump flow (CEN 2019) [mm] [in.]
A	0.31	474.5 29.6	120.0 7.5	1675.2 104.6	1.69 %	2.0 0.12	830 32.7
B	0.31	469.0 29.2	120.0 7.5	1668.9 104.2	1.75 %	1.2 0.07	785 30.9

The mechanical and thermal response of the test specimens was recorded with thermocouples embedded inside the concrete specimens (through the specimens' thickness at midspan and on the CFRP prestressing within the prestress transfer zones), and displacement gauges measuring midspan vertical displacement. Through-thickness temperature measurements at midspan were taken at eleven positions from the exposed surface for each of the specimens. Temperature measurements were also taken at several locations along the lower edge of one of the CFRP tendons within the prestress transfer zone for each of the specimens (Maluk 2014). For the work presented herein, mainly the temperature of the CFRP tendons at midspan was used for analysis. It is noteworthy that the

thermocouples at the lower edge of the CFRP tendon measured the temperature of the concrete at the surface of the tendon, rather than the temperature inside the tendon.

Experimental program — All five large-scale specimens were tested simultaneously with fire exposure from below, following a standard time-temperature curve (CEN 2020). The influence of the following design parameters was evaluated during these tests:

- concrete mixture and PP fibre dose to prevent heat-induced explosive concrete spalling (mix A and B) (refer to Table 2);
- overall specimen thickness, 45 and 60 mm, (1.77 and 2.36 in.) and concrete cover to the CFRP tendons; and
- the presence of CFRP grids to limit splitting cracking within the prestress transfer zones.

Table 2 – Test matrix for the large-scale specimens.

Specimen #	Concrete Mixture	Specimen depth [mm / in.]	CFRP grid	Time-to-failure [approx. time in minutes]	Failure mechanism
1	A	45 / 1.77	No	42	Loss of bond
2	A	45 / 1.77	Yes	13	Spalling
3	A	60 / 2.36	Yes	22	Spalling
4	B	45 / 1.77	Yes	50	Loss of bond
5	B	60 / 2.36	Yes	93	Loss of bond

Medium-scale fire tests

Test setup — A novel test method/apparatus was used for the fire tests performed at medium-scale. These tests were performed on unstressed test specimens, since the focus of these tests was a comparison of the development of splitting cracks in elements with CFRP versus steel reinforcement. The test method is called the Heat-Transfer Rate Inducing System (H-TRIS) and was conceived and developed to permit severe thermal exposures of test specimens that generate the same internal thermal gradients as would be experienced during a standard furnace test (Maluk et al. 2015). H-TRIS works by directly controlling the time-history of incident heat flux at the exposed surface of a test specimen. It uses a mobile array of propane-fired radiant panels, along with a mechanical linear motion system programmed to actively control the distance between the radiant panels and the exposed surface

of the test specimen (Figure 7); hence any desired time history of incident heat flux at the exposed surface of the test specimen can be reproduced (including simulations of essentially any standard fire resistance test in a furnace). A constant unheated overhang length of 50 mm (1.969 in.) was used for all medium-scale specimens, resulting in a heat-exposed span of only 400 mm (15.748 in.).

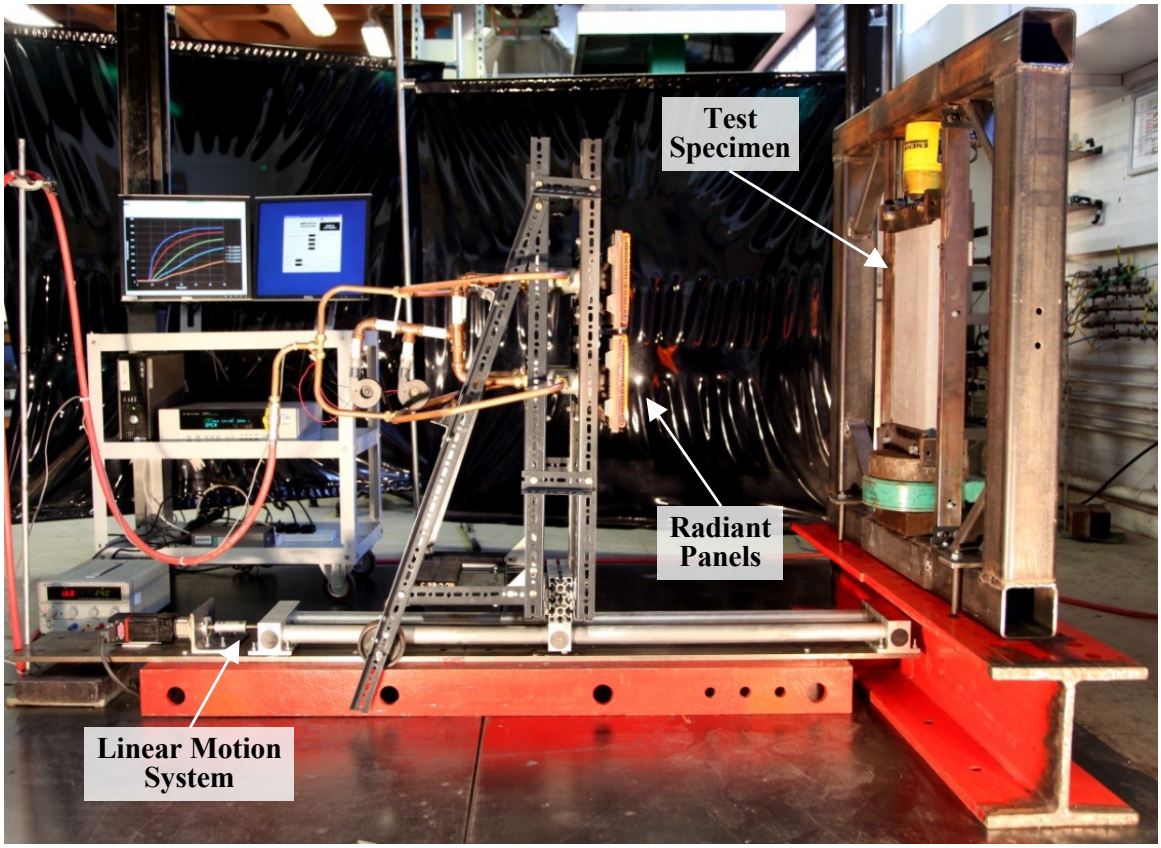

Figure 7 – Heat-Transfer Rate Inducing System (H-TRIS Mark 1) for simulating thermal exposures experienced in furnace testing.

For the current study, H-TRIS was programmed to impose a time history of incident heat flux which yielded an equivalent time history of in-depth thermal gradients to those experienced by the (essentially) identical large-scale concrete specimens that had previously been tested in the furnace tests (described above). Medium-scale fire tests were continued for a total duration of 60 minutes. The heat flux absorbed by concrete specimens during standard furnace tests (during testing of large-scale specimens) was calculated from in-depth temperature measurements recorded during the furnace tests, using a one-dimensional explicit finite difference inverse heat conduction model (see Maluk 2014). In particular, the in-depth thermal gradients measured from the furnace test of large-scale Specimen #2 were replicated. This methodology has previously been validated based on experimental data

collected during previous studies carried out with H-TRIS (Maluk et al. 2015). As for the large-scale specimens described earlier, the sides of the medium-scale specimens were fully insulated during testing. Specimens were tested under a free-to-expand and unrestrained support condition.

Experimental program — The medium-scale specimens were placed in a supporting frame and subjected to heating so as to generate the same thermal gradients as would have been experienced in the midspan region of the large-scale specimens tested in the fire testing furnace. A comparison was then made between the unstressed medium-scale test specimens (reinforced with steel or CFRP bars) tested in H-TRIS and the large-scale prestressed and loaded specimens tested in the furnace. The comparison was particularly focused on the occurrence of longitudinal splitting cracks, which were evaluated in terms of time-to-occurrence and thermal gradients within the concrete. Three medium-scale specimens were produced with unstressed CFRP and three with unstressed steel wire.

Experimental Test Results

Large- and medium-scale specimens were stored together after casting, for 1.5 months in the manufacturer's production hall. The large-scale specimens were stored indoors (ambient conditions) until testing. Concurrently, the medium-scale specimens were shipped to Edinburgh where they were stored in a conditioning room at 20°C and 80% Relative Humidity (RH) until testing. While the large-scale specimens were tested at an age of 5.2 months (with a standard fire testing furnace), the medium-scale specimens were tested at an age of 14 months (with H-TRIS).

Average moisture contents of the large-scale specimens at the time of testing, measured by mass-loss dehydration tests of control specimens were 3.6 and 3.9% by mass for mixes A and B, respectively. Accordingly, moisture contents of medium-scale specimens were 4.5 and 4.8% by mass for mixes A and B, respectively. Moisture content was measured by dehydration of control concrete samples inside ovens at 105 ºC. The medium-scale specimens likely had relatively higher average moisture contents due to the high relative humidity (80% RH) of the conditioning room.

Large-scale fire tests

Failure of specimens #1, #4, and #5 was driven by loss of bond strength within the prestress transfer zone, which resulted in structural failure at minutes 42, 50, and 93, respectively. Photographic evidence of longitudinal splitting cracks at the unexposed surface and structural failure of Specimen #4 is shown in figures 8 and 9. The first longitudinal splitting cracks at the unexposed surface of test specimens were observed near midspan, between 28 and 50 minutes from the start of the test when the temperature of the CFRP tendons at midspan was about 320-390°C (608-734°F).

Figure 8 – Longitudinal splitting cracks observed at the unexposed surface of Specimen #4 shortly before collapse.

Figure 9 – Failure (collapse) of Specimen #4 at 50' 27'' due to loss of bond strength.

Midspan vertical displacement of the specimens and temperature of CFRP tendons at midspan for specimens which failed due to loss of bond is shown in figures 10 and 11. Vertical displacement at an early stage of the test is governed by the well-known thermal bowing of the test specimens; however the observed subsequent increase in the rate of midspan deflection appears to be linked to degradation of the bond strength and the observed splitting cracking. Findings from previous studies were that the loss of bond strength during fire for a CFRP prestressed concrete element was driven by dissimilar thermal expansion, softening of the coating of the CFRP tendon, or a combination of both (Terrasi et al. 2012). Based on these findings, it was possible to correlate the midspan vertical displacement of specimens against the temperature CFRP tendons at midspan (refer to Figure 12).

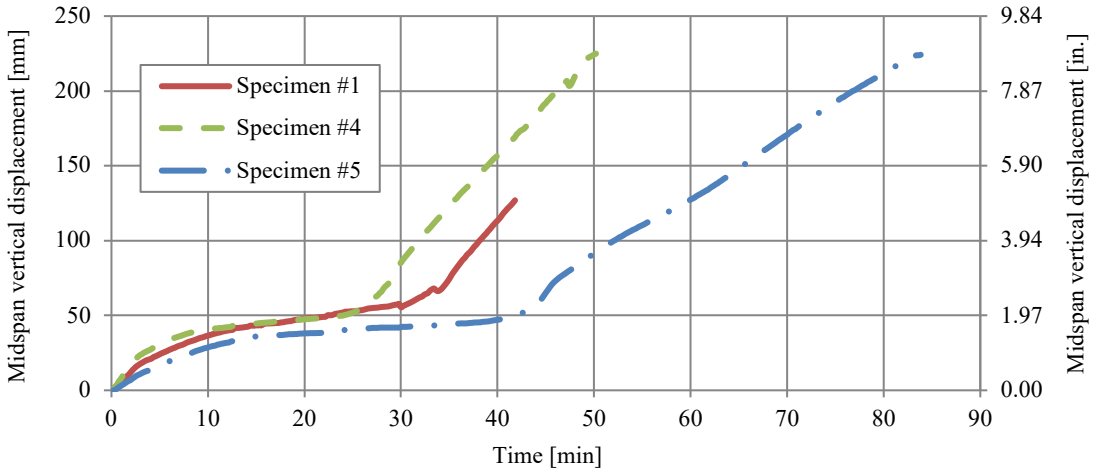

Figure 10 – Midspan vertical displacement vs. time for (specimens #1, #4, and #5).

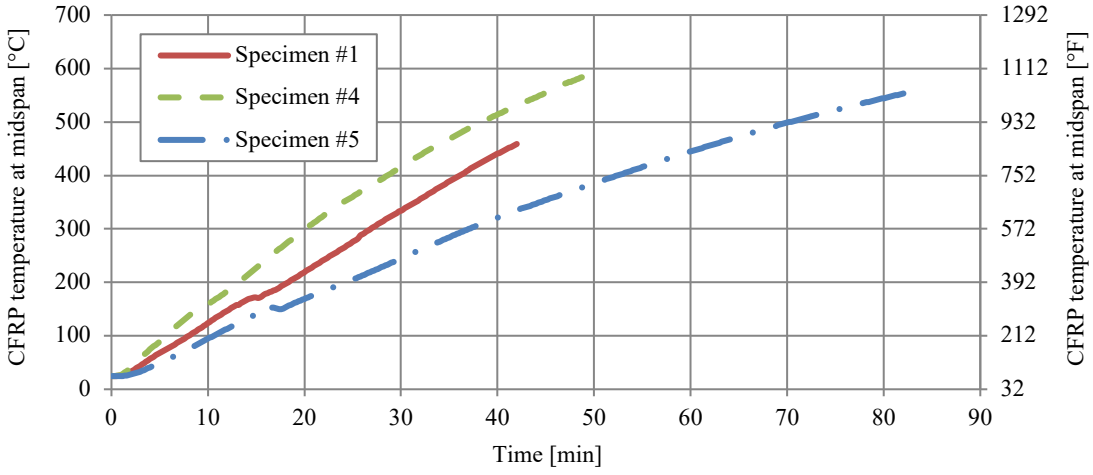

Figure 11 – CFRP temperature at midspan vs. time for (specimens #1, #4, and #5).

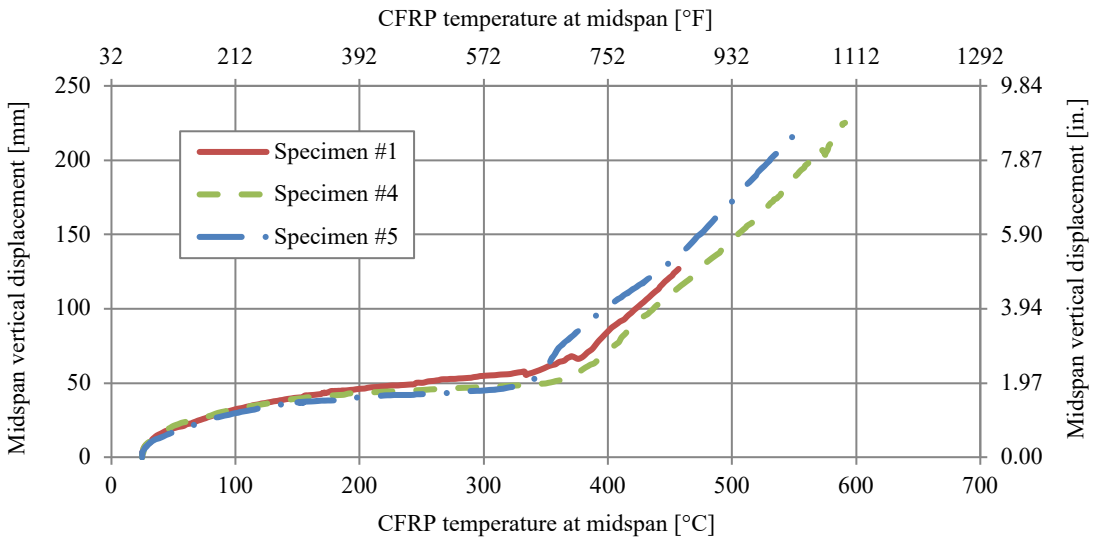

Figure 12 – Midspan vertical displacement vs. CFRP temperature at midspan (specimens #1, #4, and #5).

Failures of specimens #2 and #3, both cast from concrete Mix A, were driven by the occurrence of single explosive heat-induced concrete spalling events at minutes 12 and 22, respectively (Maluk 2014). Immediately after spalling the specimens failed suddenly. A snapshot from the video recorded during testing shows the moment at which spalling occurred for Specimen #3 (Figure 13) and highlights the violence with which pieces of concrete were expelled from the fire testing furnace.

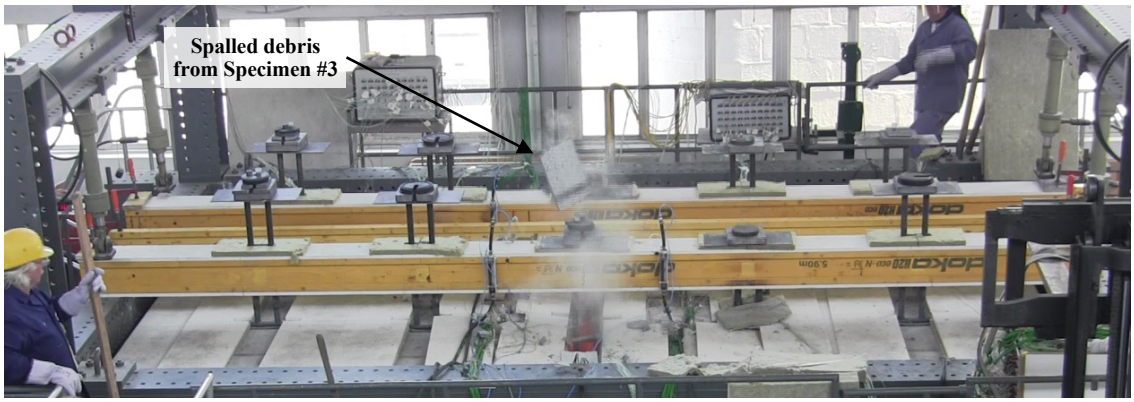

Figure 13 – Fire testing furnace, explosive spalling and imminent failure of Specimen #3 at 22’ 10’’.

Specimens #4 and #5, both cast from Mix B, showed a similarly rapid through-thickness temperature increase at midspan to that measured for specimens #2 and #3 but did not experience spalling. This suggests that for an equivalent through-thickness temperature increase (i.e. thermal exposure), the risk of heat-induced concrete spalling for specimens cast with mix B is lower than for specimens cast with mix A, and further suggests that the

shorter 6 mm (0.12 in.) PP fibres are more effective in spalling mitigation than the 3 mm (0.24 in.) fibres, even at lower doses (i.e. 1.2 versus 2.0 kg/m^3 (0.12 versus 0.07 lb/ft^3)).

Medium-scale fire test

During testing, the exposed and unexposed surfaces of the medium-scale specimens were monitored for surface longitudinal splitting cracks. Longitudinal splitting cracks at the unexposed surface of the specimens appeared at about 12 minutes from the start of the tests (refer to Table 3). Figure 14 shows photographic evidence of the longitudinal splitting cracks at the unexposed surfaces of the CFRP reinforced specimens after cooling. It is noteworthy that no surface longitudinal splitting cracks were observed at the exposed or unexposed surfaces of the steel reinforced medium-scale specimens.

Figure 14 – Unexposed surfaces of CFRP reinforced medium-scale specimens after cooling.

As in-depth thermal gradients from the large-scale Specimen #2 tested in the furnace where replicated with H-TRIS, the validity of the thermal exposure was verified by comparing in-depth temperature previously taken during testing of control specimens of practically identical dimensions (Maluk 2014). The temperature of the CFRP tendons was about 150°C (302°F) when surface cracks were first observed at

393 the unexposed surface of all the specimens tested. At the exposed surface, no visible cracks were
394 observed, however flames were observed 27-32 minutes from the start of the test, the moment at which
395 the temperature of the CFRP tendons was around 300-350°C (572-662°F).
396

397 Analysis and Discussion

398 This section describes the analysis of empirical data derived from large- and medium-scale tests; where:
399 • large-scale tests were executed on stressed concrete specimens containing CFRP tendons under sustained load;
400 and
401 • medium-scale tests were executed on unstressed concrete specimens containing CFRP tendons or steel
402 prestressing wires.

403 **Large-scale fire tests**

404

405 Recognizing that it is difficult to draw generalized conclusions on the basis of a limited number of large-scale
406 specimens simultaneously tested during a single furnace test, the following analysis can be made based on the
407 basis of the data presented herein.
408

409 To analyse the loss of bond strength and its influence in the failure mechanism observed for specimens #1, #4,
410 and #5, the midspan vertical displacement of the specimens and temperature at the lower edge of a central CFRP
411 tendon measured at midspan were compared (see figures 10 and 11). For these specimens, regardless of all design
412 parameters assessed during large-scale tests (i.e. concrete mix, overall specimen thickness, presence of CFRP
413 grids within the prestress transfer zones), a rapid increase in the rate of midspan vertical displacement was
414 observed when the temperature of the CFRP tendon at midspan was in the range of 300°C (572°F), irrespective
415 of the temperature at the prestress transfer zone (see Figure 10), before the first longitudinal splitting cracks at the
416 unexposed surface of specimens were perceived; between 28 and 50 minutes from the start of the test when
417 temperature of the CFRP tendons at midspan was about 320-390°C (608-734°F). In all cases, first cracks were
418 observed away from the prestress transfer zone, near midspan.
419

420 Furthermore, Figure 12 shows how the fire behaviour of the test specimens, specifically their midspan vertical
421 displacements, can be directly demarcated by the temperature of the CFRP tendons at midspan. This potentially

422 demonstrates a triviality of prescribing an unheated overhang length for the fire safe design of CFRP prestressed
423 concrete elements (Terrasi et al. 2012).
424
425 Specimens #4 and #5, 45 (1.77 in.) and 60 mm (2.36 in.) thick, respectively, both of which had CFRP grids in
426 their prestress transfer zones, failed when midspan temperature of the CFRP tendon was about 600°C (1112°F).
427 Specimen #1, which had no CFRP grids, failed when midspan temperature of CFRP tendons was about 450°C
428 (842°F). This indicates a possible increase in bond strength at elevated temperature provided by the presence of
429 CFRP grids in the prestress transfer zones.
430
431 Heat-induced concrete spalling and sudden failure occurred for specimens #2 and #3, both cast from Mix A, at
432 minute 12 and 22 from the start of the test, respectively (refer to Table 3). Specimen #2 suffered early failure at
433 minute 12 due to a single explosive spalling event while Specimen #1, which was virtually identical to Specimen
434 #2, failed due to loss of bond strength at minute 42 without significant spalling being observed (refer to Table 3).
435 Whilst a full analysis of the possible reasons for this cannot be included in the current paper, through-thickness
436 temperature measurements showed a more rapid temperature increase within the spalled Specimen #2 compared
437 to the non-spalled Specimen #1; due to non-uniformities of the thermal exposure experienced when tested
438 simultaneously during a single standard furnace test (Maluk 2014). Likewise, Specimen #3 (mix A), which also
439 suffered from spalling, showed more rapid temperature increases at midspan.
440 *Table 3 – Test observations for medium-scale specimens reinforced with CFRP tendons.*

Mid-scale specimen	First crack at the unexposed surface [mm:ss]	First flame at the exposed surface [mm:ss]
#1	12:03	27:50
#2	11:28	30:57
#3	11:41	31:48

441

442 **Medium-scale fire test**

443

444 These test results showed that the formation of heat-induced longitudinal splitting cracks, and eventual failure of
445 the concrete cover's capacity to provide sufficient confining action during fire, is more likely for CFRP reinforced

446 or prestressed concrete elements than for those reinforced or prestressed with steel during fire. This comparison
447 is solely on the basis of the thermo-mechanical incompatibility (i.e. differential thermal expansion) between CFRP
448 reinforcement and concrete.
449
450 As the medium-scale specimens were cast with unstressed reinforcements (CFRP or steel) and tested under a free-
451 to-expand, unrestrained condition, the effects of thermo-mechanical incompatibility were evaluated in isolation
452 from other mechanical actions encountered in large scale testing of real structural elements (e.g. bursting stresses
453 in the prestress transfer zone). The formation of longitudinal splitting cracks on unstressed, medium-scale
454 specimens occurred when the temperature of CFRP tendons was about 150°C (302°F); while for prestressed,
455 large-scale specimens, cracks formed when temperature of the CFRP tendons was around 320-390°C (608-734°F).
456 The divergence between the findings for unstressed and prestressed specimens is thought to be associated with
457 the stress superposition resulting from the sustained tensile load of the CFRP tendons. Because the diameter of
458 the tendons decreases under tensile load, due to Poisson's deformation, this potentially counteracts the heat-
459 induced expansion of the CFRP tendons during heating, as previously hypothesized by Aiello et al (2001).
460
461 These test results show that crack formation occurs more rapidly at the unexposed surface in the presence of a
462 thermal gradient, and that there is a direct dependency between crack formation and the concrete temperature (i.e.
463 the through-thickness temperatures). Flames observed at the exposed surface of the specimens, when the CFRP
464 tendons were at 300-350°C (572-662°F), are thought to be associated with pyrolysis of the CFRP's epoxy resin
465 matrix at similar temperatures observed from thermogravimetric analysis (TGA), performed on identical CFRP
466 tendons (Maluk et al. 2011).
467
468 The comparison of temperature measurements recorded for tested specimens #1, #2, and #3 evidenced the
469 influence of time-history of through-thickness temperature in the occurrence of heat-induced concrete spalling.
470 After a thorough assessment of the thermal exposure experienced by the five tested specimens (not fully presented
471 in this paper), test results showed that the risk of heat-induced concrete spalling for specimens cast including 1.2
472 kg/m^3 (0.07 lb/ft^3) of the 6 mm (0.24 in.) long PP fibres is lower than for specimens cast including 2.0 kg/m^3 (0.12
473 lb/ft^3) of the 3 mm (0.12 in.) long PP fibres.
474

Comparison with Aiello's Model

Past studies on differential thermal expansion between FRP tendons and concrete, and its influence on the structural performance of FRP reinforced (or prestressed) concrete elements during fire (e.g. Gentry and Bank 1994, Matthys 1996) have led to the development of analytical and numerical models aimed at describing this thermo-mechanical issue. A noteworthy model, aimed at describing heat-induced mechanical stresses within an FRP reinforced concrete element is presented by Aiello et al. (2001). This analytical model considers the concrete cross-section as a concrete thick-walled pipe surrounding a single tendon and subjected to the radial pressure developed at the tendon-concrete interface.

Aiello et al.'s (2001) model is based on an axisymmetric treatment of the thermal stress problem and simplifies the confining action within a reinforced (or prestressed) concrete element. The model refers to a single rebar within the concrete cover, and without transverse reinforcement. Aiello's (2001) model predicts the occurrence of heat-induced splitting cracks in FRP reinforced concrete by modelling the influence of a temperature increase (ΔT) on the radial stresses (σ_r) in the concrete cover (see Figure 15). The model is described in three discrete temperature steps (see Figure 16): (a) the temperature before initiation of a crack at the FRP-concrete interface (once the tensile strength of concrete is overcome), (b) the temperature between initiation of the crack until the crack reaches the outer radius of the cylinder, and (c) the temperature after the crack reaches the outer radius of the cylinder.

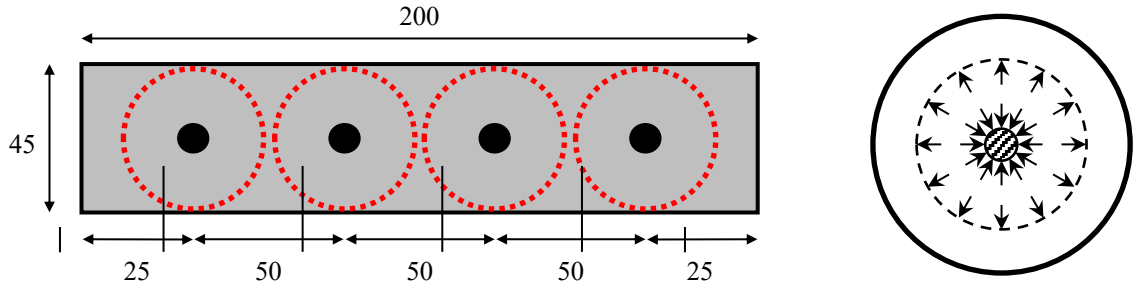

Figure 15 – Tendon and concrete effective areas for a 45mm thick specimen, and radial stresses acting at the tendon-concrete interface under temperature increase (Maluk et al. 2010).

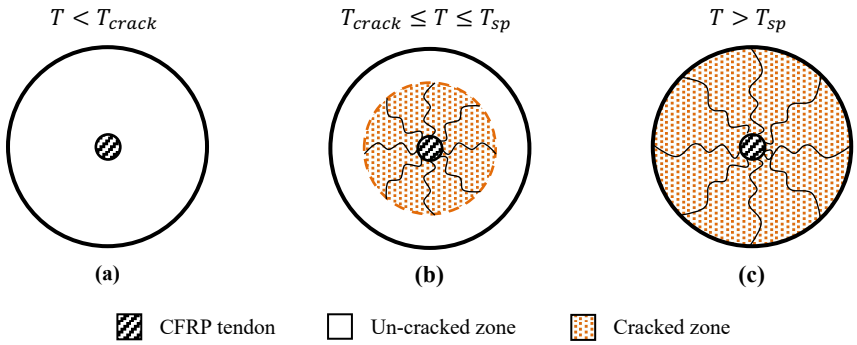

498

499 Figure 16 – Three temperature ranges of thermal incompatibility assumed in Aiello et al.'s (2001) model (Maluk
500 et a. 2010) – (a) temperature before initiation of a crack at the FRP-concrete interface, (b) temperature between
501 initiation of a crack and the crack reaching the outer radius of the cylinder, and (c) temperature after a crack
502 reaches the outer radius of the cylinder.

503

504 The model (Aiello et al. 2001) is based on the following assumptions:

505 • the temperature of the FRP tendon and concrete increases uniformly (i.e. there is no through-thickness thermal
506 gradient within tested specimens; this is clearly not the case in the current tests);

507 • a temperature dependent elastic modulus and tensile strength of concrete can be used as inputs; and

508 • each FRP tendon is treated independently, meaning that the clear spacing between two adjacent tendons is
509 sufficient to avoid the occurrence of horizontal splitting cracks at the tendon level; this is a reasonably good
510 assumption for the specimens tested herein (refer to Figure 15).

511

512 A thorough description of Aiello et al.'s (2001) model is avoided here, and only a brief description is given. The
513 mechanical stress at the tendon-concrete interface (see Figure 16) is given by:

514

515 $$\sigma_T(T) = \frac{[\,\alpha_{tendon}(T) - \alpha_c(T)\,]}{\frac{1}{E_c(T)}\left[\ln\frac{r_{crack}}{r_{tendon}} + \frac{r_c^2 + r_{crack}^2}{r_c^2 - r_{crack}^2} + \upsilon_c\right] + \frac{1}{E_{tendon}(T)}[1 - \upsilon_{tendon}]} \cdot (T - T_{amb}) \quad (1)$$

516

517 Due to the axisymmetric of the formulation, the radial (σ_r) and circumferential (σ_θ) stresses at a generic point in
518 the concrete cover, at a distance "x" from the centre of the reinforcement, are given by the following equations:

519

520 $$\sigma_r(x) = \frac{r_{tendon}^2}{r_c^2 - r_{tendon}^2}\left(1 - \frac{r_c^2}{x^2}\right)\sigma_T(T) \quad (2)$$

$$\sigma_\theta(x) = \frac{r_{tendon}^2}{r_c^2 - r_{tendon}^2}\left(1 + \frac{r_c^2}{x^2}\right)\sigma_T(T) \quad (3)$$

A comparison of Aiello et al.'s (2001) model and the findings from the experiments on large-scale and medium-scale fire tests herein is shown below. Temperature dependent mechanical properties for concrete, CFRP, and steel, used as inputs for the analytical model, were taken from previous studies and available design guidelines. The mechanical properties of concrete were defined as:

- The compressive ($f_c = 90\ MPa$) and tensile ($f_{ck} = 5.6\ MPa$) strengths at ambient temperature were taken from Maluk (2014).
- The strain (ε_{c1}) corresponding to f_c was taken from the Eurocodes (CEN 2004b).
- The Elastic modulus was defined using the 'secant method' described by ACI (2019).
- The Poisson's ratio ($v_c = 0.2$) was assumed after Logan et al. (2009)
- Reduction factors (k_c) for concrete properties at elevated temperatures were taken from the Structural Eurocodes (CEN 2004b).

The coefficients of thermal expansion for concrete $\alpha_c(T)$, CFRP (transversal) $\alpha_{CFRP}(T)$, and steel $\alpha_s(T)$ used are shown in Figure 4. The elastic modulus in the transverse direction ($E_{tendon} = 6\ GPa$) and Poisson's ratio ($v_{tendon} = 0.35$) for the CFRP tendon were assumed after Aiello et al. (2001). Although not considered in the model presented herein, it's noteworthy that the elastic modulus of the CFRP tendon in the transverse direction will inevitably (and considerably) decrease at elevated temperatures (Schneider et al. 1981); although potentially relevant, the influence of this assumption is not analysed in the current paper. The model was applied to replicate the thermo-mechanical behaviour of the 45 and 60 mm (1.77 and 2.36 in.) thick specimens reinforced with CFRP tendons or steel from the current study, under two conditions which bracket the likely outcome under a thermal gradient in the concrete:

1) The temperature of the FRP tendon and concrete increases *uniformly* – this is a first order approximation modelling the conditions at the fire exposed surface of the specimen.

549 2) The temperature of the FRP tendon increases while the temperature of concrete *remains at ambient*
550 temperature – first order approximation modelling the conditions at the unexposed surface of the specimen.
551
552 Results from the model were plotted to indicate the crack tip location against the temperature of the CFRP tendon
553 (see Figure 17). This indicates the temperature at which the crack first initiated (red circle) and the temperature at
554 which the crack reached the outer radius of the concrete (green rhombus).

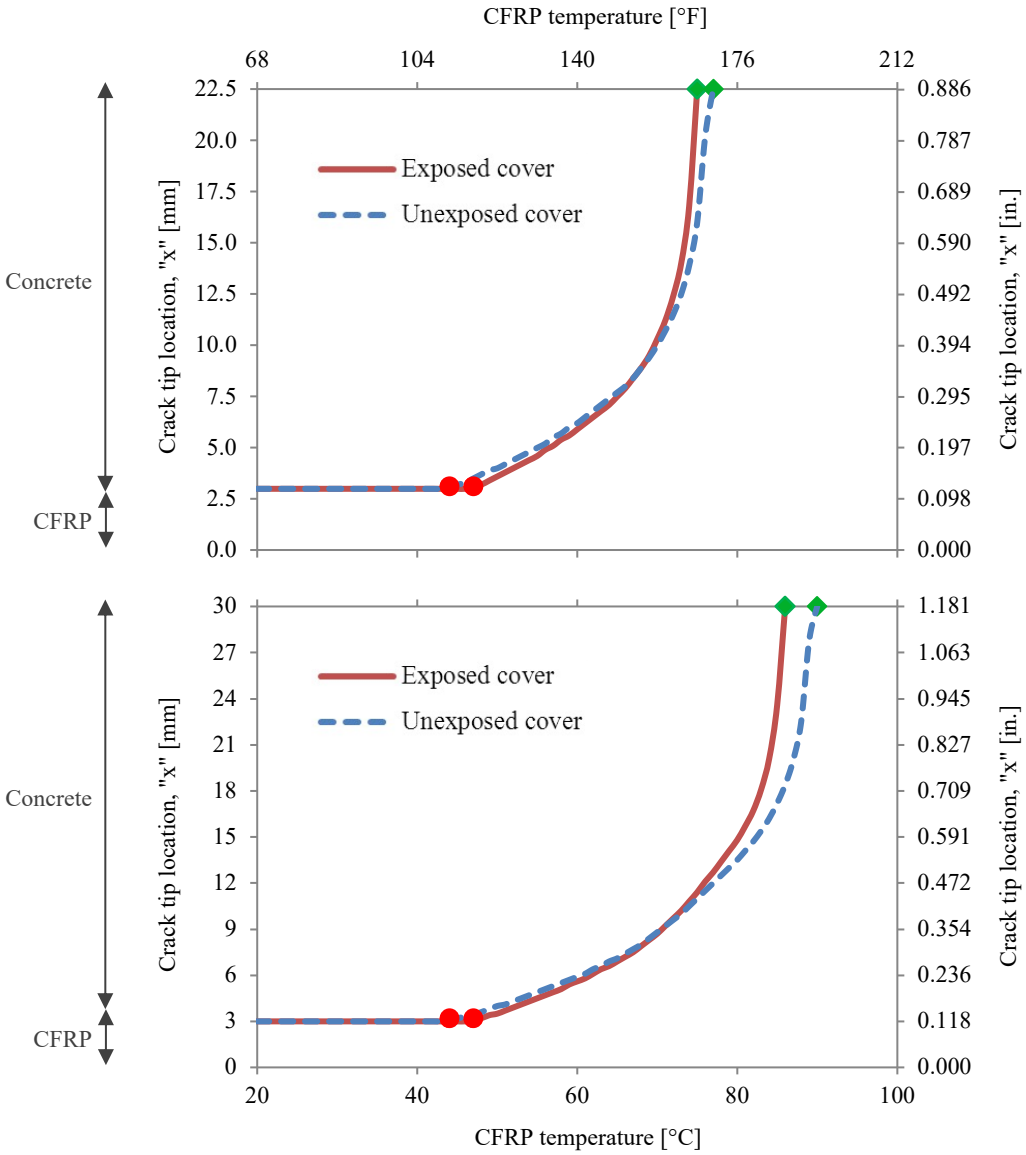

555
556 *Figure 17 – Correlation between predicted crack propagation and temperature of the CFRP tendon at the exposed*
557 *and unexposed cover for a 45 mm (1.77 in.) (top figure) and 60 mm (2.36 in.) (bottom figure) thick specimens.*

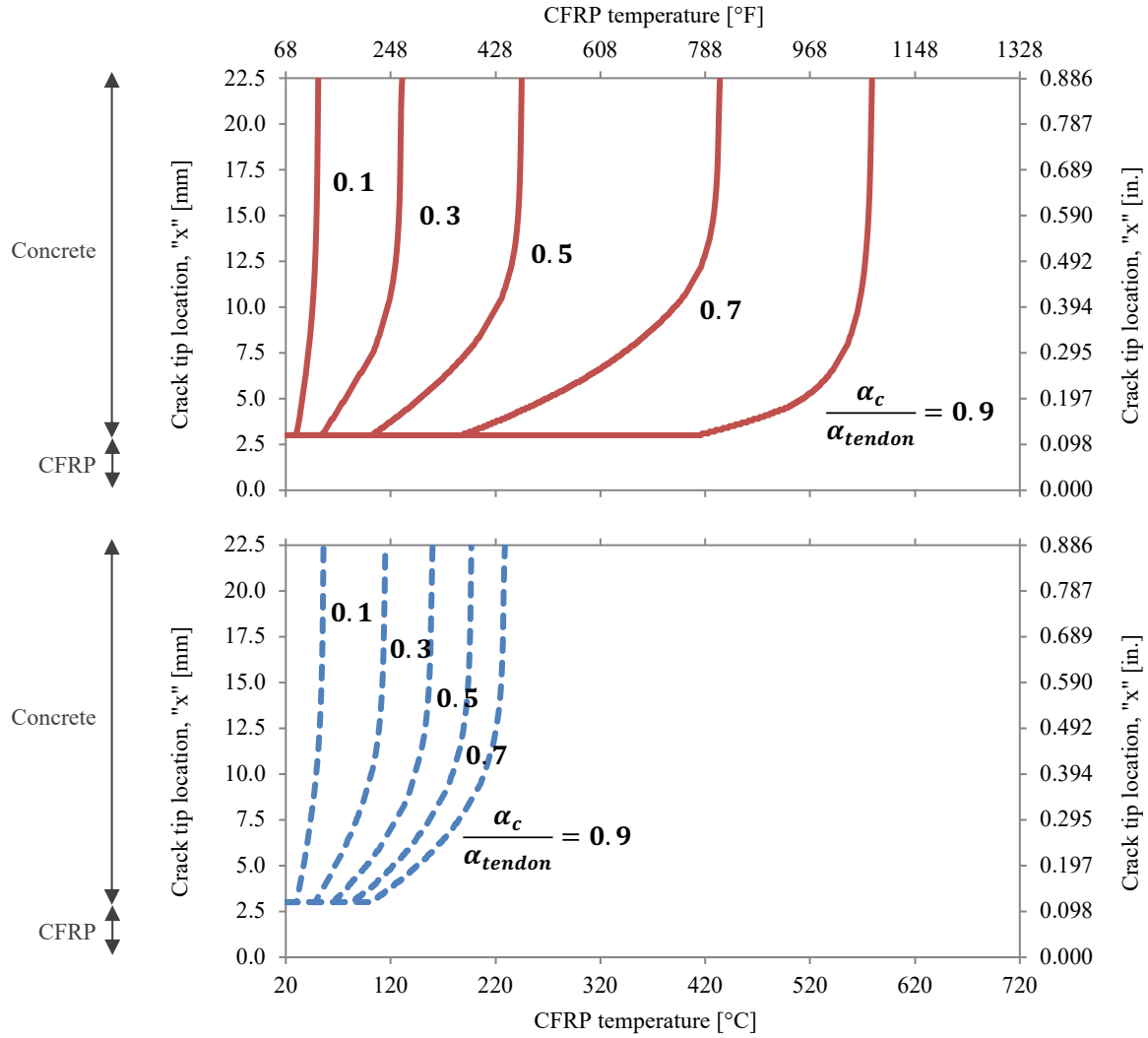

Figure 18 – Predicted correlation between crack propagation and temperature of the CFRP tendon for the exposed (top figure) and unexposed (bottom figure) cover conditions of a 45 mm (1.77 in.) thick specimen.

As shown in Figure 17, crack initiation at the tendon-concrete interface is independent of the amount of the concrete cover initiating when the CFRP tendon is at 44°C (111°F) for the unexposed cover and at 47°C (117°F) for the exposed cover. Crack initiation is slightly influenced by the temperature of the concrete, simulating the conditions of the exposed or unexposed concrete cover. As the crack propagates from the CFRP tendon, unstable cracking spreads as the tip of the crack reaches the outer surface of the concrete cover.

For the condition in which CFRP and concrete are uniformly heated – simulating the exposed cover – the crack reaches the outer surface of the cover when the temperature of the CFRP is 75 and 86°C (167 and 187°F), for 45 and 60 mm (1.77 or 2.36 in.) thick specimens, respectively (see Figure 17). For the conditions in which only the

571 CFRP is heated – simulating the unexposed cover – the crack reaches the outer surface of the cover when the
572 temperature of the CFRP is 77 and 90°C (171 and 194°F), for 45 and 60 mm (1.77 or 2.36 in.) thick specimens,
573 respectively.
574
575 The comparison with large-scale and medium-scale tests described above shows the 'conservative' results given
576 by the analytical model (i.e. surface cracking was observed for significantly higher temperature to those resulting
577 from modelling). For medium-scale, unstressed specimens, cracks at the unexposed surface where first observed
578 when temperature of the CFRP tendon was about 150°C (302°F), while the model predicts that cracking of the
579 surface for a 45 mm (1.77 in.) thick specimens occurs when the CFRP tendon is at 75°C (167°F). The above
580 divergence between experiments and theory could be explained by the precision of visual observation for crack
581 formation at the surface and selection of material properties used as input in the model.
582
583 The sensitivity of the model to coefficient of the thermal expansion used as an input is shown in Figure 18. In this
584 instance, the coefficient of the thermal expansion for CFRP was calculated as a ratio of that defined for concrete
585 (α_c/α_{tendon}). This figure shows, as expected, that Aiello et al.'s (2001) model is highly sensitive to the
586 differential thermal expansion between the CFRP and the concrete. The novelty of this analysis is falls in the
587 difference in the results obtained when replicating exposed and unexposed concrete covers:
588
589 • when assuming a relatively low differential thermal expansion between CFRP and concrete (i.e. a high value
590 of α_c/α_{tendon}), crack initiation and cracking of the outer surface of the cover are highly influenced by the
591 conditions given by an exposed or unexposed cover; on the other hand,
592
593 • when assuming a relatively high differential thermal expansion between CFRP and concrete (i.e. a low value
594 of α_c/α_{tendon}), crack initiation and cracking of the outer surface of the cover is only slightly influenced by
595 the conditions given by an exposed or unexposed concrete cover.
596
597 The above highlights the importance of accurately gauging the coefficient of thermal expansion for the two
598 materials (internal reinforcement and concrete), and the high sensitivity of Aiello et al.'s (2001) model for the
599 coefficient of thermal expansion assumed. The visual assessment of crack initiation at the heated and unheated

surfaces is only qualitative, and findings from Aiello et al.'s (2001) indicated crack formation at the heated and unheated surfaces happening almost for the same temperature of the CFRP tendon.

The CFRP tendons used by SACAC and supplied by Prince Fiber Tech from Dronten NL was the result of an evaluation of available pultrusion diameters back in 2008 (which means available pultrusion dies for CFRP being 4 mm, 5.4 mm and 6.5 mm diameter tendons) at Prince Fiber Tech in Dronten NL.
I needed enough cross section for having a reasonable prestress force per tendon (i.e. 23 – 27.5 kN) and an as small as possible diameter to avoid CTE and prestress transfer cracks when pretensioning, considering that we wanted to keep the cover at 20 mm approx.
With a 6.5 mm tendon I observed (back in 2001!) splitting cracks at prestress transfer of P = ca. 40 kN when c = 20 mm, though I moved to 5.4 mm and got no cracks when transferring up to 27.5 kN per tendon.
We shall tell the reader that SACAC evaluated the at the time available pultrusion bars and came to the conclusion that a diameter of >= 6.5 mm (next size/diameter available after 5.4 mm) gave prestress transfer cracks of the concrete cover, which they wanted to minimize and keep around 20 mm to reduce the elements weight.

Conclusions and Recommendations

The study presented herein has shown the results of fire tests carried out on large-scale, prestressed and medium-scale, unstressed thin-walled specimens incorporating CFRP tendons. The following conclusions can be drawn on the basis of the findings and analysis presented:

- Whilst during fire tests on large-scale specimens, no attempt was made to individually gauge the influence of softening of the coating of the CFRP tendon versus the dissimilar thermal expansion between CFRP and concrete, large-scale test results confirmed that at a combination of both mechanisms is relevant. The fire-behaviour of test specimens can be directly demarcated by the temperature of the CFRP tendons at midspan (see Figure 12), confirming the insignificance of prescribing an unheated overhang length for the fire safe design of CFRP prestressed concrete elements.

- Based on the findings from the large-scale fire tests, irrespective of all design parameters assessed in this study (e.g. section thickness, presence of CFRP grids, concrete mix), loss of bond strength started when the

630 temperature of the CFRP tendons at midspan was in the range of 300°C (572°F). The presence of CFRP grids
631 within the prestress transfer zones showed an increase in the time-to-failure of the tested specimens which
632 failed due to loss of bond strength. While specimens with CFRP grids failed when midspan temperature at the
633 lower edge of a cantered CFRP tendon was about 600°C (1112°F), this occurred at 450°C (842°F) for the
634 specimen without CFRP grids in the prestress transfer zone.
635
636 • Based on the findings from the medium-scale fire tests, the formation of heat-induced longitudinal splitting
637 cracks, and eventual failure of the concrete cover's capacity to provide sufficient confining action, is more
638 likely for FRP reinforced or prestressed concrete elements than for those reinforced or prestressed with steel
639 during fire. This is due at least partly, as demonstrated with the tests presented herein, to the differential
640 thermal expansion between FRP and concrete. As test specimens in this study were cast with unstressed
641 internal reinforcement (CFRP or steel), and tested under a free-to-expand unrestrained condition, the
642 influences of differential thermal expansion have been evaluated in isolation from other mechanical actions
643 encountered in large scale testing of real structural elements (e.g. bursting stresses in the prestress transfer
644 zone).
645
646 • The limitations of available analytical models currently used to describe the formation of heat-induced
647 longitudinal splitting cracks in FRP reinforced (or prestressed) concrete elements are mainly driven by the
648 material properties (e.g. CTE or elastic modulus of CFRP and concrete at elevated temperatures), used as input
649 and the assumption of a uniform temperature increase within the concrete specimen, rather than by the extreme
650 thermal gradients that are likely to be experienced during fire exposures in buildings (or during fire tests).
651
652 • Many aspects of bond performance at elevated temperature remain poorly understood and require additional
653 investigation for FRP reinforced or prestressed elements which are bond critical. Additional testing and
654 modelling are required to better understand these and other complexities of the behaviour of CFRP prestressed
655 concrete elements during fire.
656
657 Finally, the thermal incompatibility between CFRP and concrete has a detrimental effect on the bond behaviour
658 between CFRP tendons and concrete; therefore, a detrimental influence in the structural performance of these
659 systems during fire. The text has been modified accordingly. It is hoped that findings from this study reveal some

660 of the irrationality in using standard furnace tests for investigating the fire performance of highly optimized CFRP
661 prestressed concrete structural elements. As herein, the high risk of heat-induced concrete spalling and the
662 complexities associated with structural failure due to loss of bond strength capacity, both of which are relevant to
663 the fire behaviour of such optimized structural elements during fire, are difficult to investigate with testing a small
664 number of large-scale specimens. A better understanding of the response of these elements is needed before they
665 can be designed and implemented with confidence; this is unlikely to be achieved by performing standard furnace
666 tests.
667
668 The H-TRIS testing method is able to accurately quantify the thermal conditions encountered in a large-scale fire
669 resistance test, with high precision and repeatability, and at negligible economical and temporal cost compared to
670 traditional furnace testing.

671 **Notation**

672 α_{tendon} = coefficient of thermal expansion of bar in transversal direction

673 α_c = coefficient of thermal expansion of concrete

674 α_s = coefficient of thermal expansion of steel

675 f_c = compressive strength for concrete

676 f_{ck} = tensile strength for concrete

677 ε_{c1} = strain corresponding to f_c

678 k_c = reduction factor for concrete properties at elevated temperature

679 T = temperature of the tendon and/or concrete

680 $T_{ambient}$ = temperature at ambient conditions

681 T_{crack} = temperature at which the crack is initiated at the tendon-concrete interface

682 T_{sp} = temperature at which the crack reaches the outer surface of the concrete cylinder

683 r_{tendon} = radius of tendon

684 r_c = radius of concrete cylinder

685 r_{crack} = radius of crack concrete cylinder (i.e. location of the tip of the crack)

686 x = generic point in the concrete cover from the centre of the reinforcement

687 σ_T = mechanical stress at the tendon-concrete interface

688 σ_r = radial stresses in concrete

689 σ_θ = circumferential stresses in concrete

690 v_c = Poisson's ratio of concrete

691 v_{tendon} = Poisson's ratio of tendon

692

693 **Data Availability Statement**

694 All data, models, and code generated or used during the study appear in the submitted article.

695 **References**

696 Abdalla H. (2006). Concrete Cover Requirements for FRP Reinforced Members in Hot Climates. *Composite*
697 *Structures*, 73 (1), 61-69.

698 ACI (2015). Guide for the Design and Construction of Concrete Reinforced with FRP Bars (ACI 440.1R-15)",
699 *American Concrete Institute*, US, 88pp.

700 ACI (2019). Building Code Requirements for Structural Concrete and Commentary (ACI 318-19). *American*
701 *Concrete Institute*, US, 624pp.

702 Aiello M.A. (1999). Concrete Cover Failure in FRP Reinforced Beams under Thermal Loading. *Journal of*
703 *Composites for Construction*, 3 (1), 46-52.

704 Aiello M.A., Focacci F., and Nanni A. (2001). Effects of Thermal Loads on Concrete Cover of Fibre-Reinforced
705 Polymer Reinforced Elements: Theoretical and Experimental Analysis. *ACI Materials Journal*, 98 (4),
706 332-339.

707 ASTM (2019). Standard Test Method for Linear Thermal Expansion of Solid Materials by Thermomechanical
708 Analysis (ASTM E831). *American Society for Testing and Materials (ASTM)*, 5 pp.

709 Balafas I. and Burgoyne C.J. (2012). Economic Design of Beams with FRP Rebar or Prestress. *Magazine of*
710 *Concrete Research*, 64 (10), 885-898.

711 Bisby L.A., Green M.F. and Kodur V.K.R. (2005). Response to Fire of Concrete Structures that Incorporate FRP.
712 *Progress in Structural Engineering and Materials*, 7 (3), 136–149.

713 Bisby L.A. and Kodur V.K.R. (2007). Evaluating the Fire Endurance of Concrete Slabs Reinforced with FRP
714 Bars: Considerations for a Holistic Approach. *Composites Part B: Engineering*, 38 (5-6), 547-558.

715 Burgoyne C.J. (1997). Rational Use of Advanced Composites in Concrete (keynote lecture), *Proceedings of the*
716 *3rd International Symposium on Non-Metallic (FRP) Reinforcement for Concrete Structures*, Sapporo,
717 Japan, Vol. 1, 75-88.

718 CEN (2004a). Eurocode 2: Design of Concrete Structures – Parts 1-1: General Rules and Rules for Buildings (EN
719 1992-1-1:2004). *European Committee for Standardization*, Brussels, 230 pp.

720 CEN (2004b). Eurocode 2: Design of Concrete Structures – Parts 1-2: General rules – Structural Fire Design (EN
721 1992-1-2:2004). *European Committee for Standardization*, Brussels, 100 pp.

722 CEN (2019). Eurocode: Testing Fresh Concrete – Part 8: Self-compacting Concrete – Slump-flow Test (EN
723 12350-8:2019). *European Committee for Standardization*, Brussels, 10 pp.

724 CEN (2020). Eurocode: Fire Resistance Tests – Part 1: General Requirements (EN 1363-1:2020). *European*
725 *Committee for Standardization*, Brussels, 54 pp.

726 Clarke J.L. (1993). *Alternative Materials for the Reinforcement and Prestressing of Concrete*. Glasgow, UK:
727 Taylor & Francis. 224 pp. ISBN: 9780203487679

728 CNR (2006). Guide for the Design and Construction of Concrete Structures Reinforced with Fibre-reinforced
729 Polymer Bars (CNR-DT 203/2006). *National Research Council*, Rome, Italy, 39 pp.

730 Gentry T.R. and Bank, L.C. (1994). Application of FRP reinforcement in structural precast concrete. *Proceedings*
731 *of the 3rd Infrastructure: A New Materials and Methods of Repair conference – ASCE*, Vancouver, Canada,
732 575–582.

733 Harmathy T.Z. and Lie T.T. (1970). Fire Test Standard in the Light of Fire Research. *Fire Test Performance –*
734 *ASTM Special Technical Publication 464*, 85-97.

735 Katz A. (1999). Bond Mechanism of FRP Rebars to Concrete. *Materials and Structures*, 32 (10), 761-768.

736 Logan A., Choi W., Mirmiran A, and Rizkalla S.H. (2009). Short-Term Mechanical Properties of High-Strength
737 Concrete. *ACI Materials Journal*, 106 (5), 413-418.

738 Maluk C., Bisby L., Krajcovic M., and Torero J.L. (2019). Heat-Transfer Rate Inducing System. *Fire Safety*
739 *Journal*, 105, 307-319.

740 Maluk C. (2014). Development and application of a novel test method for studying the fire behaviour of CFRP
741 prestressed concrete structural elements, *Ph.D. thesis*, The University of Edinburgh, UK.

742 Maluk C., Bisby L., Terrasi G., Hugi E., and Green M. (2011). Bond Strength Degradation for CFRP and Steel
743 Reinforcing Bars in Concrete at Elevated Temperature. *American Concrete Institute Special Publication*
744 *on Advances in Fire Design of Concrete Structures (ACI SP-297)*, 36 pp.

745 Masmouid R., Zaidi A., and Gérard P. (2005). Transverse Thermal Expansion of FRP Bars Embedded in Concrete.
746 *Journal of Composites for Construction*, 9 (5), 377-387.

747 Matthys S., De Schutter G., and Taerwe L. (1996). Influence of Transverse Thermal Expansion of FRP
748 Reinforcement on the Critical Concrete Cover. *Advanced Composite Materials in Bridges and Structures,*
749 *Society for Civil Engineering, Montreal*, pp. 665-672.

750 Mehta P.K. (1997). Durability – Critical Issues for the Future. *Concrete International*, 19 (7), 27-33.

751 Schneider H., Menges G., and Peulen J. (1981). Beitrag zur experimentellen und theoretischen Ermittlung der
752 Elastizitätskenngrössen von CFK-Laminaten (A contribution to the experimental and theoretical
753 investigation of the elasticity constants of CFRP laminates). *Proceedings of the Federation of Reinforced*
754 *Plastics Conference (Industrievereinigung Verstärkte Kunststoffe Konferenz)*, Freudenstadt, Germany.

755 Seica M.V. and Packer J.A. (2007). FRP Materials for the Rehabilitation of Tubular Steel Structures, for
756 Underwater Applications. *Composite Structures*, 80 (3), 440-450.

757 Terrasi G.P. (2007). Prefabricated Thin-Walled Structural Elements Made from HPC Prestressed with Pultruded
758 Carbon Wires. *Proceedings of the 8th International Symposium on Fibre Reinforced Polymer*
759 *Reinforcement for Concrete Structures*, Patras, Greece, 10 pp.

760 Terrasi, G.P. (1998). Mit Kohlenstoffasern vorgespannte Schleuderbetonrohre (CFRP prestressed spun concrete),
761 *Ph.D. thesis*, ETH, Zurich, Switzerland.

762 Terrasi G., Bisby L., Barbezat M., Affolter C., and Hugi, E. (2012). Fire Behavior of Thin CFRP Pretensioned
763 High-Strength Concrete Slabs. *Journal of Composites for Construction*, 16 (4), 381–394.

List of Figures

List of Tables